Short communication

The effect of interconnect rib size on the fuel cell concentration polarization in planar SOFCs

Zijing Lin, J.W. Stevenson, M.A. Khaleel[*]

Laboratory Engineering Mechanics Group, Pacific Northwest National Laboratory, P.O. Box 999, Mail stop K2-18, Richland, WA 99352, USA

Abstract

The gas transport in the porous electrode is treated by a phenomenological approach such that the gas concentration at the three-phase boundary (TPB) region is the additive superposition of that transported from the source, i.e. the gas channels. With plausible approximations and elemental algebra, analytical expressions are obtained to estimate the effects of ribs on the concentration polarization of planar fuel cell operations. It is shown that the model can closely reproduce the experimental concentration polarization curve for small and medium current density (up to about 2 A/cm^2), providing a simple and effective method for engineering application. The concentration polarization caused by the presence of a rib is discussed and the concentration profiles with varying rib widths are illustrated. In connection with the electrical resistance, the determination of the optimal rib width for minimizing the overall polarization is also shown.
© 2003 Elsevier Science B.V. All rights reserved.

Keywords: Fuel cell; Concentration polarization; Gas transport; Rib design; Analytical model

1. Introduction

Solid oxide fuel cells offer great potential for high efficiency, environmentally benign electric energy generation. There is a great deal of research on solid oxide fuel cells generally, especially on new material systems and on electrochemical performance of the cell, or membrane-electrode assembly (MEA). Planar-type designs have received much attention because they potentially offer higher power density relative to the tubular-type SOFC, which is ascribed to the low electrical resistance due to shorter current paths. In particular, a very thin electrolyte film can be used in an anode-supported SOFC, drastically reducing the ohmic resistance and enabling operation at intermediate temperature [1–3]. However, relatively little of the literature concentrates on such critical technical issues as the system-level layout of the layers and stacks [4–6].

Under ideal conditions (i.e. pure hydrogen fuel and low fuel utilization), single cells with optimized materials can yield power densities on the order of 0.5–1 W/cm^2 or higher. For practical applications, however, multiple cells must be connected in series by interconnect material to form a fuel cell stack. Small channels, which are often formed in the interconnect material, are commonly used to carry the fuel and air gas flow. The ''ribs'', which separate and define the flow channels, make direct contact with the electrodes. In designing the layer architecture, there is a tradeoff that must be considered between the rib and channel sizes. On one hand, wider ribs and ribs covering bigger fraction of the cell area may reduce the interface resistance to current flow by increasing the electrode–interconnect contact area and reducing the current path through the possibly high resistance electrode material. Hence, such ribs will give a better conduction of the electrical current and reduce ohmic losses. On the other hand, the chemical species do not diffuse as well underneath wide ribs. Narrow ribs are needed to facilitate more uniform distribution of reactive gases across the area of the electrolyte surface and thus to promote electrochemical performance. The implication of the tradeoff to the cell performance is very significant. It was reported that the maximum power output was only 871 mW/cm^2 for the combination of 4 mm channels and 4 mm ribs, while that for 1 mm channels and 2 mm ribs was 1930 mW/cm^2 for some proton exchange membrane (PEM) fuel cells [7]. Clearly, a designer must decide how to configure a channel network to optimize the cell performance.

The general approach in discussing the rib effects is to map out the transportation process in the case of rib presence, starting from the known parameters when ribs are

* Corresponding author. Tel.: +1-509-375-2438; fax: +1-509-375-6605.
E-mail address: moe.khaleel@pnl.gov (M.A. Khaleel).

absent. A rigorous analysis requires a 3D model of the porous electrode joined with the interconnect rib and electrolyte sheet. The gas transportation path determines the diffusion polarization and electrochemical performance, and the electrical path determines the ohmic polarization. The optimal rib design can then be determined. While such 3D analysis is undoubtedly useful in revealing the details of the complex interaction of competing factors, the results are difficult to generalize because they are usually dependent on a great number of design and operational parameters. As such, the approach is usually unable to provide easy-to-use design guidance to the broad fuel cell engineering society.

The purpose of the present work is to derive some simple guidelines for estimating the effects of the interconnect rib area on the concentration polarization as a function of the different physical and geometrical parameters involved. This will provide a more complete basis for optimizing the stack repeat unit geometry—especially the shape and dimensions of the interconnect. The results of this paper assist the designer in understanding how channel sizing affects gas uniformity for the system by formulating the model in a dimensionless framework, enabling a generalization of the results in terms of one characteristic diffusion parameter and one dimensionless geometry parameter.

2. Concentration polarization model

The maximum usable work at constant temperature and pressure is the free energy change of a reaction, $G = G_0 + (RT/2F) \ln(P_{H_2} P_{O_2}^{1/2} / P_{H_2O})$, where G_0 is the free energy change at the standard state (for simplicity, we use H_2 fuel in the discussion, though the principle is of general applicability). It can be easily seen that the fuel gas pressures contribute to the Nernst potential by $[RT/2F] \ln[P_{H_2}/P_{H_2O}]$. At gas channels, the fuel gas pressures are, respectively, $P_{H_2}^0$ and $P_{H_2O}^0$. These correspond to the maximum work available for external work if the electrochemical reaction were taking place at the channels; however, the reaction takes place at the three-phase boundary (TPB) (i.e. gas–electrolyte–electrode). The gas pressures at TPB are, respectively, P_{H_2} and P_{H_2O} due to diffusion resistance (loss). The maximum work available is then only $G_0 + RT \ln[P_{H_2}/P_{H_2O}]$, and the Nernst potential is less than the ideal case by $[RT/2F] \ln\{P_{H_2}^0 P_{H_2O}/P_{H_2} P_{H_2O}^0\}$. The loss is due to the anode concentration polarization. Similarly, resistance to the oxidant diffusion from cathode gas channel to the corresponding TPB region causes the cathode concentration polarization.

Suppose a point X at the TPB has coordinate $(x, y, 0)$, a point Q is at gas channel–electrode interface with (u, v, l_e), where l_e is the electrode thickness. Without loss of generality, we can assume the channels are along the y-direction. Let L_0 be the penetration distance, characterizing the maximum distance the gas can diffuse from the channel before it is consumed by the cell reaction. From a phenomenological point of view, the gas concentration at X is the summation of

those diffused from sources of all Q's at the electrode–channel surfaces and within the penetration distance from X:

$$P_x = \int dP_x = \int C(u, v) \, dA_Q, \qquad (1)$$

where $dA_Q = du\, dv$ is the area represented by Q, and the 3D diffusion source function, C, is expected to be dependent on the gas pressure at Q and the distance between Q and X. Integration along the y-direction (channel) can be carried out implicitly by using average property of C and reducing the 3D diffusion form to an in-plane diffusion expression:

$$P_x = \int dP_x = \int_{x-L_0}^{x+L_0} B(u)F(u) \, du \qquad (2)$$

Here, $B(u)$ is the in-plane source function, while $F(u)$ takes a value of 1 when u is inside channels and 0 when u is inside the ribs. It can be expected that $B(u)$ decays roughly exponentially with the distance between X and Q due to the nature of concentration diffusion. One can quite reasonably write

$$B = \alpha e^{-cdi} \qquad (3)$$

so that the gradient of the source function is balanced by the flow resistance (proportional to the current density) in accordance with Darcy's law of diffusion in a porous medium [8]. Here, c is a constant characterized by the electrode diffusivity, best determined by the experimental data and $d = \sqrt{l_e^2 + (u - x)^2}$ is the distance between u and x. The effective current density in the channel is i, and $i = i_0/(1 - f)$, where i_0 is the current density without a rib present, and f is the fraction of rib width to the rib–channel width, as seen by the point X. That is, the effective channel gas flux (proportional to i) should be $1/(1 - f)$ times that of no-rib flux due to smaller cross-section available for gas transport with rib presence. Assuming no capillary forces, $P_x = P_0$, when $i = 0$, and it is found $\alpha = P_0/[2L_0(1 - f)]$. In other words, the source function is

$$B = \left(\frac{P_0}{2L_0(1 - f)}\right) e^{-cdi} \qquad (4)$$

By integrating Eq. (2) for the anode, one can obtain the H_2 pressures at the TPB with a single undetermined parameter, "c", when the electrode thickness and the current density are specified. The best fit to the experimental data without rib presence provides the desired "c". With the specified "c", integration of Eq. (2) with rib presence would allow us to discuss the rib effects on concentration polarization.

Applying a similar approach to the cathode side, one can obtain O_2 pressure at the TPB. Notice that there is in general no correlation between "c" for H_2 and "c" for O_2 due to different microstructures and materials. However, it is reasonable to expect "c" to be inversely proportional to the diffusion coefficient, and one may set $c(O_2) = (1/2) c(H_2)[D(H_2-H_2O)/D(O_2-N_2)][\varepsilon(H_2)\tau(O_2)/\varepsilon(O_2)\tau(H_2)] \approx 2[\varepsilon(H_2)\tau(O_2)/\varepsilon(O_2)\tau(H_2)]c(H_2)$. The first factor, 1/2, is due to only half the amount of O_2 as of H_2 needing to be transported. Here, ε/τ is the porosity/tortuosity factor; their

inclusion changes the factor "2" to some different value and does not change the qualitative results described below for anode-supported fuel cells, where cathode diffusion polarization is small compared with that of the anode and will not be discussed explicitly.

Eq. (2) generally requires numerical integration. Though numerical integration poses no difficulties in principle, an analytical approach is preferred for ease of analysis and is discussed below. Assuming the electrode thickness is relatively small compared with L_0, we may approximate $d = [l^2 + (u - x)^2] \simeq |u - x|$. This approximation is reasonable for a thin electrode or low to medium current density, where the penetration distance is expected to be large, as it is in the case we are focused on. For high current density, such approximation is not expected to be very good; however, we will show that this is not a serious limitation for practical purposes.

When there is no rib present, one can integrate Eq. (2) easily if d is replaced with $|u - x|$ and gives the TPB H_2 pressure as

$$P_{H_2} = P_{H_2}^0 \frac{(1 - e^{-A_0})}{A_0} \tag{5}$$

where $A_0 = cL_0i_0$.

For H_2O pressure at the TPB, which is higher than that at the channel–electrode surface for H_2O transport out of the TPB, a treatment similar to that for H_2 can be used. The resulting expression depends on c_{H_2O}, which is in principle different from that for H_2 due to different diffusivities. Because H_2 is lighter and moves faster than H_2O, the total pressure of H_2O at TPB should be slightly higher than that at the channel–electrode surface for an equal counter-current of H_2 and H_2O to occur. However, this adds undue complexity with an additional parameter and is not necessary for our discussion, which is to provide easy-to-use guidelines for estimating the rib effects. Therefore, we will simply follow Kim et al. [2] and assume $P_{H_2} + P_{H_2O} = P$, where P is the total pressure of H_2 and H_2O in the gas channel. Therefore, the TPB H_2O pressure can be obtained by

$$P_{H_2O} = P_{H_2O}^0 + P_{H_2}^0 - P_{H_2}$$
$$= P_{H_2O}^0 \left\{ 1 + \frac{P_{H_2}^0}{P_{H_2O}^0} \left[1 - \frac{(1 - e^{-A_0})}{A_0} \right] \right\} \tag{6}$$

The anode concentration polarization is then

$$\eta(\text{diffusion}, A_0)$$
$$= -\frac{RT}{2F} \ln \left\{ \frac{(1 - e^{-A_0})/A_0}{1 + (P_{H_2}^0/P_{H_2O}^0)[1 - (1 - e^{-A_0})/A_0]} \right\} \tag{7}$$

One can find the parameter c by fitting Eq. (7) to experimental anode polarization data. Rewriting the usual anode polarization form,

$$\eta_a(\text{diffusion}) = -\frac{RT}{2F} \ln \left(\frac{1 - (i/i_{as})}{1 + (P_{H_2}^0/P_{H_2O}^0)(i/i_{as})} \right) \tag{8}$$
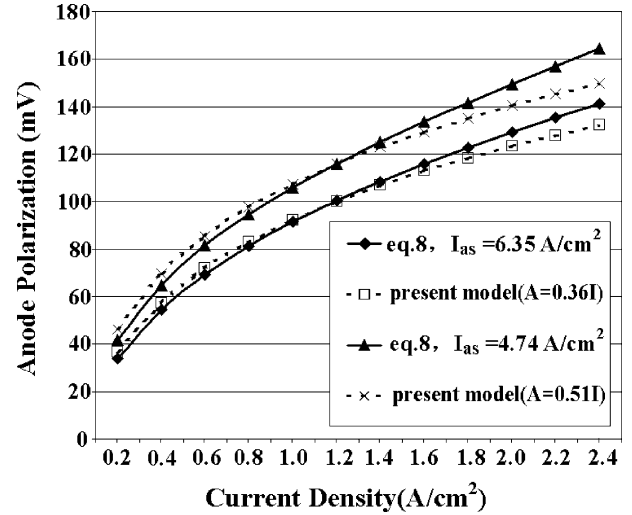

Fig. 1. Comparison of present concentration polarization model with Eq. (8) and experimental parameters.

Virkar et al. [1] and Kim et al. [2] found the best fit to their experimental data as $i_{as} = 4.74$–6.35 A/cm² for intermediate working temperature ($T = 700$–800 °C), where i_{as} is the anode limiting current. Although the anode polarization expression of Eq. (7) is very different from that of Eq. (8), using $A/i = 0.36$ and 0.51 (cm²/A), respectively, for $i_{as} = 4.74$ and 6.35 A/cm², Eq. (7) can fit Eq. (8) reasonably well. Fig. 1 shows the comparison of Eqs. (7) and (8) for the two representative cases. As can be seen, the fit is good for small and medium current density. The difference is less than 5 mV for current density up to about 2 A/cm². For larger current density, the fit is not good due to a much faster increase of Eq. (8) than that of Eq. (7). This is a consequence of the approximation made in calculating distance, d, where the anode thickness is neglected. However, it is not a serious limitation because the fit is good for working current densities. Therefore, Eq. (7) is a useful expression in describing anode polarization.

3. Rib effects

Due to the smaller cross-section available for gas transport, the ribs lengthen the effective gas diffusion distance, resulting in increased concentration polarization. In particular, if the rib width is larger than the diffusion penetration distance, there will be appreciable underused or even unused areas under the rib shadows, reducing the cell performance substantially. On the other hand, if the rib width is smaller than the penetration distance, the gas concentration at the TPB is expected to be uniform, and the cell should perform relatively well. Therefore, from the concentration polarization point of view, narrow ribs are preferred over wide ribs if the ratio of rib width to that of channel width is fixed.

3.1. Narrow rib effect

Assuming uniform channel spacing, the rib width is a, and the channel width is $d - a$; $f = a/d$ is the fraction of the rib width in the width of rib–channel pair, d. Without loss of generality, we may choose the TPB location as $0 < x < d$. If $x < a$, the point is under the rib shadow, while that for $x > a$ is under the channel. The left-most channel within the penetration distance is at $N_1 < 0$; the right-most channel is at $N_2 > 0$ (N_2 is expected to be $|N_1|$ or $|N_1| \pm 1$). The channels' ranges are $[jd + a, (j + 1)d]$, and the ribs' ranges are $(jd, jd + a), j \in [N_1, N_2]$. For cases with very narrow ribs, $L_0 = Nd = N_2 d = -N_1 d \gg d$, Eq. (2) can be written as

$$P_x = \left[\frac{P_0}{2L_0(1-f)}\right] \sum_{j=N_1}^{N_2} \int_a^d e^{-A(|jd+u-x|/L_0)}\,du$$

$$= \left[\frac{P_0}{2L_0(1-f)}\right] \left[\sum_{j=-N}^{-1} \int_a^d e^{A(jd+u-x)/L_0}\,du \right.$$

$$\left. + \sum_{j=1}^N \int_a^d e^{-A(jd+u-x)/L_0}\,du + \int_a^d e^{-A|u-x|/L_0}\,du\right] \quad (9)$$

After some algebra, we have

$$P_x = \left[\frac{P_0}{2A(1-f)}\right]\left\{\frac{[1-e^{(f-1)A/N}](1-e^{-A})}{1-e^{-A/N}}\right.$$

$$\times [e^{-(x/d)(A/N)} + e^{-((d-x+a)/d)(A/N)}] + \delta(a-x)$$

$$\times [e^{-((a-x)/d)(A/N)} - e^{-((d-x)/d)(A/N)}] + \delta(x-a)$$

$$\left. \times [2 - e^{((a-x)/d)(A/N)} - e^{-((d-x)/d)(A/N)}]\right\} \quad (10)$$

Considering very narrow rib limit ($N \gg 1$), Eq. (10) reduces to

$$P_{H_2} = P_{H_2}^0 \frac{(1-e^{-A})}{A} \quad (11)$$

where $A = cL_0 i = cL_0 i_0/(1-f) = A_0/(1-f)$. This expression has the same form as the no-rib case except that the effective current density should be used. In other words, the no-rib expression is a special case of the narrow rib expression with $f = 0$. The gas concentration is uniform in the TPB region whether the area is under channels or under ribs. The uniformity is due to the diffusion penetration distance being much larger than the rib width. In fact, numerical results show that, in practice, uniformity is achieved with any $N > 1$. Therefore, Eq. (11) is a representative expression for all cases where the diffusion penetration distance is larger than the combined width of a rib and a channel.

As the above derivation shows, the net effect of narrow ribs is to replace A_0 with $A = A_0/(1-f)$ in Eq. (5), where f is the fraction of rib width to the width of the rib–channel pair. The difference between using A and A_0 in Eq. (7) is the extra anode polarization caused by the narrow ribs:

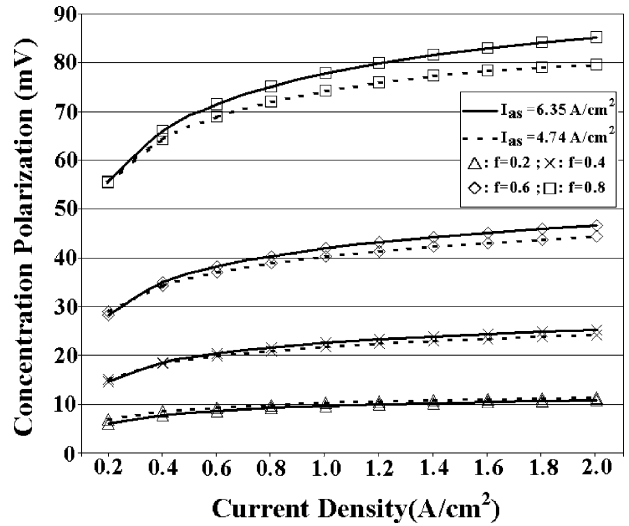$$\eta_{rib}(\text{diffusion}, A) = \eta(\text{diffusion}, A) - \eta(\text{diffusion}, A_0) \quad (12)$$

Fig. 2. Rib contribution to the concentration polarization as a function of the rib width fraction, f.

Fig. 2 shows the extra concentration polarization with $f = 0.2$, 0.4, 0.6, and 0.8 for various current densities.

For anode-supported fuel cells, the cathode concentration polarization is expected to be much smaller than that of the anode. The extra concentration polarization caused by ribs in the cathode side is also expected to be small and is not discussed explicitly here.

3.2. Wide rib effect

When the penetration distance is about half the rib width or smaller, the rib effect on the concentration polarization is expected to be the most significant due to significant under-utilized area under ribs. In the following, we focus on cases with $L_0 \le d$. In such cases, the possible integrals involved in calculating Eq. (2) are

$$I_1 = \int_{x-L_0}^0 e^{A(u-x)/L_0}\,du\,\delta(L_0-x)\delta(x-L_0+d-a)$$

$$= \frac{L_0}{A}(e^{-Ax/L_0} - e^{-A})\delta(L_0-x)\delta(x-L_0+d-a) \quad (13a)$$

Here, the step functions are used to indicate that I_1 appears only if $x < L_0$ and $x - L_0 > -d + a$.

$$I_2 = \int_{-d+a}^0 e^{-A|u-x|/L_0}\,du\,\delta(-d+a-x+L_0)$$

$$= \frac{L_0}{A}[e^{-Ax/L_0} - e^{-A(d-a+x)/L_0}]\delta(-d+a-x+L_0) \quad (13b)$$

$$I_3 = \int_a^d e^{-A|u-x|/L_0}\,du\,\delta(a-x+L_0)\delta(x+L_0-d)$$

$$= \frac{L_0}{A}\{\delta(a-x)[e^{-A(a-x)/L_0} - e^{-A(d-x)/L_0}]$$

$$+ \delta(x-a)[2 - e^{A(a-x)/L_0} - e^{-A(d-x/L_0)}]\}$$

$$\times \delta(a-x+L_0)\delta(x+L_0-d) \quad (13c)$$

$$I_4 = \int_a^{x+L_0} e^{-A|u-x|/L_0}\,du\,\delta(a-x+L_0)\delta(x+L_0-a)$$

$$\times\,\delta(d-x-L_0) = \frac{L_0}{A}\{\delta(a-x)[e^{-A(a-x)/L_0}-e^{-A}]$$

$$+\,\delta(x-a)[2-e^{A(a-x)/L_0}-e^{-A}]\}\delta(a-x+L_0)$$

$$\times\,\delta(x+L_0-a)\delta(d-x-L_0) \tag{13d}$$

$$I_5 = \int_{x-L_0}^{d} e^{-A|u-x|/L_0}\,du\,\delta(x-L_0-a)\delta(x+L_0-d)$$

$$= \frac{L_0}{A}(2-e^{A(d-x)/L_0}-e^{-A})\delta(x-L_0-a)\delta(x+L_0-d)$$

$$\tag{13e}$$

$$I_6 = \int_{x-L_0}^{x+L_0} e^{-A|u-x|/L_0}\,du\,\delta(x-L_0-a)\delta(d-x-L_0)$$

$$= \frac{L_0}{A}(2-2e^{-A})\delta(x-L_0-a)\delta(d-x-L_0) \tag{13f}$$

$$I_7 = \int_{d+a}^{x+L_0} e^{-A|u-x|/L_0}\,du\,\delta(x+L_0-d-a)$$

$$= \frac{L_0}{A}(e^{-A(d+a-x)/L_0}-e^{-A})\delta(x+L_0-d-a) \tag{13g}$$

With the above integrals, the gas pressure is found by simple summation:

$$P_x = \alpha\sum_{j=1}^{7} I_j$$

Despite their lengthy appearance, the above analytical expressions contain only elemental functions and can be easily implemented in a spreadsheet. As an example, Fig. 3 shows the concentration distribution for $L_0 = d/4$ and the rib width $= (0.2, 0.4, 0.6)d$ for the current density of 1 A/cm². The concentration distributions with no ribs and with narrow ribs are also shown for comparison. The average concentrations fo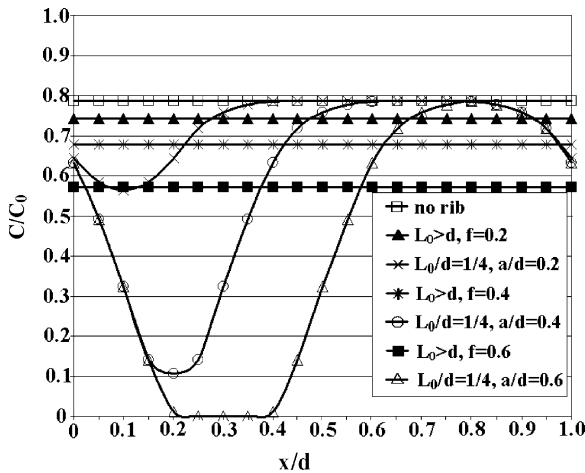r the rib widths of 0.2, 0.4, and 0.6 are 98, 87 and 74%, respectively, of that for the corresponding narrow ribs. Clearly, wide ribs cause higher concentration polarizations, and designs with narrow ribs are, in general, preferred if the percentage of rib width is fixed.

4. Rib optimization

The optimal rib designs depend on balancing the rib effects on the concentration polarization and the electrical resistance. The electrical resistance includes both the ohmic resistance of the rib material and the contact resistance between the ribs and the electrodes. Typically, the contact resistance is much higher than the ohmic resistance of the rib material [7,9–13]. The overall area electrical resistance of the ribs can be written as $R_{rib} = \beta/f$, where f is the rib width fraction as discussed above and typical β-values are 10–100 mΩ cm² [7]. Without the contact resistance, β is usually smaller than 1 mΩ cm² [9,10]. For simplicity, we will only discuss the narrow rib scenario. More general discussion and characterization of the rib design will be reported in another paper.

Fig. 4 shows the variation of the overall overpotential caused by ribs with f for three representative β-values of 2, 10, and 50 mΩ cm² for current density of 1 A/cm² and operating temperatures of 800 °C and $I_{as} = 5.65$ A/cm². The minimum overall polarization indicates the best overall rib width design for the specified operating temperature and target current density. Though small rib width fraction is intuitively favored, the optimal rib width depends strongly on the electrical resistance. The optimal rib width fraction is, respectively, $f = 0.2, 0.35, 0.6$, for $\beta = 2, 10, 50$ mΩ cm². The optimal rib width is similar for $T = 800$ °C and $T = 700$ °C. The higher the electrical resistance caused by ribs, the larger is the rib width fraction preferred. Small rib width fraction ($f \leq 0.2$) is preferred only when the contact resistance is very small. In most cases, the rib width fraction of $\geq 1/3$ is expected.

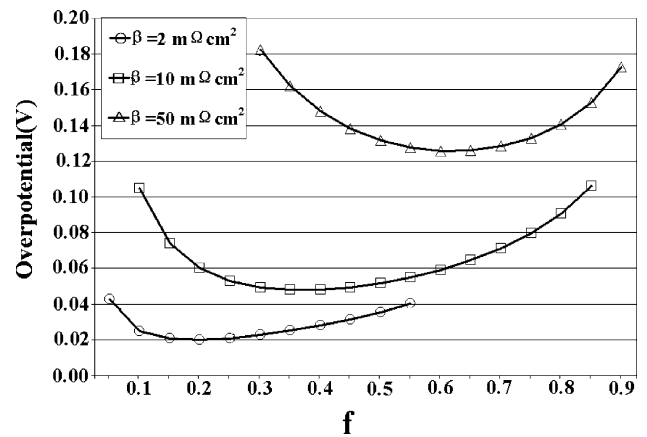Fig. 3. Fuel concentration distribution for $L_0/d = 1/4$ with various rib widths.

Fig. 4. Overall rib polarizations by varying rib width fractions for three rib electrical resistances.

5. Summary

We have provided a simplified phenomenological model for the concentration polarization. The model fits the experimental data well for any reasonable working current density. Using the model, the effect of rib size on the concentration polarization can be obtained analytically, and the model provides an easy-to-use guidance for optimizing the rib–channel layout. The following conclusions are based on the results from the analytical solutions:

- When the rib width is small compared with that of the characteristic penetration distance, the gas concentration is uniform. The concentration polarization with the rib presence takes the same form as that without ribs except that the effective current density should be used.
- When the rib width is comparable or larger than that of the characteristic penetration distance, non-uniform gas concentration results and the average concentration is smaller than that of the narrow ribs for the corresponding rib width fraction, resulting in higher concentration polarization. Therefore, narrow ribs are preferred over wide ribs for a chosen rib width fraction.

The optimal rib design is obtained by minimizing the overall ohmic and concentration polarization of the ribs. The optimal rib width is affected significantly by the electrical resistance. The higher the rib electrical resistance, the larger the rib width faction should be. For realistic electrical resistance, the rib width fraction is expected to be between 1/3 and 2/3 of the channel width.

References

[1] A.V. Virkar, J. Chen, C.W. Tanner, J.W. Kim, Solid State Ionics 131 (2000) 189.
[2] J.W. Kim, A.V. Virkar, K.Z. Fung, K. Mehta, S.C. Singhal, J. Electrochem. Soc. 146 (1999) 69.
[3] S. de Souza, S.J. Visco, L.C. De Jonghe, J. Electrochem. Soc. 144 (1997) L35.
[4] R.J. Kee, P. Korada, K. Walters, M. Pavol, J. Power Sources 109 (2002) 148.
[5] M.A. Khaleel, K.P. Recknagle, Z. Lin, J.E. Deibler, L.A. Chick, J.W. Stevenson, SOFC-VII, in: H. Yokokawa, S.C. Singhal (Eds.), The Electrochemical Society Proceedings Series, Pennington, NJ, PV2001-16, 2001.
[6] A. Solheim, SOFC-IV, in: S.C. Singhal, H. Iwahara (Eds.), The Electrochemical Society Proceedings Series, Pennington, NJ, PV1993-4, 1993.
[7] P.L. Hentall, J.B. Lakeman, G.O. Mepsted, P.L. Adcock, J.M. Moore, J. Power Sources 80 (1999) 235.
[8] A. Reizes, Transport Phenomena in Heat and Mass Transfer, Elsevier, Amsterdam, 1992.
[9] H. Yakabe, T. Ogiwara, M. Hishinuma, I. Yasuda, J. Power Sources 102 (2001) 144.
[10] J.R. Ferguson, J.M. Fiard, R. Herbin, J. Power Sources 58 (1996) 109.
[11] R.J. Boersma, N.M. Sammes, J. Power Sources 63 (1996) 215.
[12] M. Iwata, T. Hikosaka, M. Morita, T. Iwanari, K. Ito, K. Onda, Y. Esaki, Y. Sakaki, S. Nagata, Solid State Ionics 132 (2000) 297.
[13] H. Yakabe, M. Hishinuma, M. Uratani, Y. Matsuzaki, I. Yasuda, J. Power Sources 86 (2000) 423.